Interleukin-1β Folding between pH 5 and 7: Experimental Evidence for Three-State Folding Behavior and Robust Transition State Positions Late in Folding[†]

John M. Finke and Patricia A. Jennings*

Department of Chemistry and Biochemistry, University of California, San Diego, La Jolla, California 92093-0359

Received May 28, 2002; Revised Manuscript Received August 9, 2002

ABSTRACT: The thermodynamic stability and folding kinetics of the all β-sheet protein interleukin-1β were measured between 0 and 4 M GdmCl concentrations and pH 5−7. Native interleukin-1β undergoes a 3.5 kcal/mol decrease in thermodynamic stability, $\Delta G_{NU}^{H_2O}$, as pH is increased from 5 to 7. The native state parameter m_{NU}, measuring protein destabilization/[GdmCl], remains constant between pH 5 and 7, indicating that the solvent-exposed surface area difference between the native state and unfolded ensemble is unchanged across this pH range. Similarly, pH changes between 5 and 7 decrease only the thermodynamic stability, ΔG^{H_2O}, and not the *m*-values, of the kinetic intermediate and transition states. This finding is shown to be consistent with transition state configurations which continue to be the high-energy configurations of the transition state in the face of changing stability conditions. A three-state folding mechanism U $\rightleftarrows$ I $\rightleftarrows$ N is shown to be sufficient in characterizing IL-1β folding under all conditions studied. The *m*-values of refolding transitions are much larger than the *m*-values of unfolding transitions, indicating that that the fast, T_2 (U $\rightleftarrows$ I), and slow, T_1 (I $\rightleftarrows$ N), transition states are highly similar to the intermediate I and native state N, respectively. Many of the folding properties of interleukin-1β are shared among other members of the β-trefoil protein family, although clear differences can exist.

A number of previous protein folding studies have been conducted on the all-β-sheet protein, interleukin-1β (IL-1β)[1] (*1*−*3*). Recent experimental work has revealed that IL-1β refolding kinetics can be fit adequately with two exponential processes and that a discrete intermediate ensemble is present during refolding (*4*, *5*). This experimental work is in good agreement with the observation of a discrete folding intermediate in the folding simulation of a IL-1β, using only a C_α atomic polypeptide representation of the polypeptide and a Go force field (*6*). However, a complete thermodynamic analysis of kinetic states has not been conducted to confirm whether a three-state (U $\rightleftarrows$ I $\rightleftarrows$ N) kinetic model is consistent with the thermodynamic parameters obtained from equilibrium studies.

In many respects, the folding properties of IL-1β are consistent with many proteins. The thermodynamic stability, *m*-value of equilibrium unfolding, and heat capacity are within the range expected for a protein of its size (*7*). However, the primary difference between IL-1β and other proteins is that IL-1β folding is particularly slow, both in terms of intermediate formation as well as formation of the native state. With the exception of certain two-state folding proteins, most proteins initially fold to intermediate states at rates faster than can be resolved with stopped-flow mixing methods (<5 ms). Recent work using ultrarapid mixing and temperature jump methods has indicated that these initial folding events typically occur in the microsecond time range (*8*−*10*). By contrast, the U $\rightleftarrows$ I transition in IL-1β folding is in the millisecond time range and completely accessible with stopped flow kinetic measurements. Interestingly, other members of the β-trefoil family studied, aFGF, bFGF, and hisactophilin, also appear to form an initial intermediate from the unfolded ensemble (U $\rightleftarrows$ I) on a millisecond/second time scale (*11*−*14*). However, IL-1β intermediate formation is much more distinct kinetically than other β-trefoil proteins since, in IL-1β, the rates of the U $\rightleftarrows$ I and I $\rightleftarrows$ N steps differ by 2 orders of magnitude (*4*). Also, the time constants for β-trefoil native state formation (τ = 10−1000 s), with the possible exception of hisactophilin (τ = 0.003 s), appear unusually slow compared to those of other proteins (*11*−*14*).

This study reports measurements of IL-1β thermodynamic and kinetic folding parameters between pH 5 and 7. The first goal of this study is to determine whether the three-state kinetic folding mechanism can model IL-1β folding under a variety of pH conditions. The three-state kinetic folding model will be tested by determining if transition state energies and *m*-values, measured from kinetic studies, can reproduce the thermodynamic stability and *m*-values, measured from equilibrium studies. The second goal is to determine the impact pH changes between 5 and 7 have on the properties of intermediates and transition states in the IL-1β folding pathway. A final objective is to use the folding

[†] This work supported by a Hellman Faculty Fellowship (P.A.J.), a Sloan Fellowship (P.A.J.), NIH Grant GM54038 (P.A.J.), P.H.S. Grant CA09523 (J.M.F.), La Jolla Interfaces In Science Interdisciplinary Training Program (J.M.F.), and the Burroughs Welcome Fund (J.M.F.)

* Corresponding author. Address: University of California at San Diego, 9500 Gilman Drive, La Jolla, CA 92093-0359. Phone: (858) 534-6417. Fax: (858) 534-7042. E-mail: pajennin@ucsd.edu.

[1] Abbreviations: IPTG, isopropyl-β-D-thiogalactopyranoside; PMSF, phenylmethyl sulfonyl fluoride; KPO_4, potassium phosphate; EDTA, ethylenediaminetetraacetic acid; DTT, dithiothreitol; βme, 2-mercaptoethanol; Tris-HCl, tris(hydroxymethyl)aminomethane hydrochloride; NH_4OAc, ammonium acetate; MES, 2-(4-morpholino)-ethane sulfonic acid; GdmCl, guanidine hydrochloride; GdmSCN, guanidine thiocyanate; FPLC, fast protein liquid chromatography; SASA, solvent accessible surface area; SDS−PAGE, sodium dodecyl sulfate-polyacrylamide gel electrophoresis; IL-1β, interleukin-1β.

10.1021/bi026197k CCC: $22.00
Published on Web 11/19/2002

measurements to evaluate structural properties of the unfolded, intermediate, and transition state ensembles in the IL-1β folding pathway.

MATERIALS AND METHODS

Expression and Purification of IL-1β and K97I. The gene encoding wild-type IL-1β was subcloned into a pET 24-d vector (Novagen) and transformed into *E. coli* BL21(DE3) cells. Cells were grown in LB to an OD_{600} of 0.8, and protein expression was induced with IPTG at a final concentration of 1 mM. Rifampicin was added 45 min after induction to a final concentration of 0.1 mg/mL. Three hours after induction, cells were harvested by centrifugation at 10 000*g* for 30 min.

Purification of IL-1β was based on Meyers et al. (*15*) but with a number of modifications. Cells were resuspended in 10 mM KPO_4, 0.2 mM EDTA, 5 mM DTT, and 1 mM PMSF at pH 8.0 and then lysed by sonication at 4 °C, followed by centrifugation at 4300*g* for 30 min. Soluble IL-1β in the supernatant was made 80% saturated in ammonium sulfate and then precipitated by centrifugation as above. The pellet was then dissolved in buffer A (25 mM NH_4OAc, 2 mM EDTA, and 1 mM βme at pH 4.5) and dialyzed overnight in buffer A at 4 °C.

The dialysate was centrifuged as above, filtered, and applied to a Resource S cation exchange column (Pharmacia) equilibrated in buffer A. IL-1β was eluted in a 40 column volume linear gradient of 25−240 mM NH_4OAc, pH 4.5, at a flow rate of 3 mL/min. Purity was judged to be greater than 95% as assessed by SDS−PAGE. Protein concentrations were calculated using an experimentally determined $\epsilon_{280} = 11.26\ mM^{-1}\ cm^{-1}$ (*16*). Purified protein was dialyzed extensively into a constant ionic strength buffer containing 100 mM MES, 50 mM Tris−HCl, 50 mM acetic acid for all experiments discussed. The IL-1β concentration was 6 μM for all experiments discussed.

Equilibrium Fluorescence pH and GdmCl Titrations. Equilibrium unfolding and pH titrations were measured using intrinsic tryptophan fluorescence emission intensity. Protein samples were diluted to varying final pH and GdmCl concentrations and equilibrated overnight. Fluorescence spectra were acquired on a Fluoromax-2 spectrofluorimeter (SPEX, Edison, NJ). Fluorescence emission was measured as total intensity over the 300−450 nm emission range after excitation at 293 nm.

Manual-Mixing Fluorescence. Unfolding experiments were initiated by addition of native IL-1β stock into a cuvette to final GdmCl concentrations ranging from 2 to 5 M. Refolding experiments were initiated by dilution of unfolded IL-1β at 2.2 M GdmCl to final GdmCl concentrations ranging from 0.2 to 1.8 M. The kinetics of folding reactions with relaxation times greater than 10 s were measured by the time dependent change in fluorescence emission at 343 nm (slit 1 mm) while exciting at 293 (slit 1 mm) nm using a Fluoromax-2 spectrofluorimeter equipped with a Neslab RTE-111 temperature controller.

Stopped-Flow Fluorescence. Folding reactions with relaxation times less than 10 s were monitored with an Applied Photophysics SX.17MV (Applied Photophysics, London) stopped-flow unit with a path length of 0.1 cm. Refolding experiments were initiated by a 1:10 dilution of unfolded IL-1β at 2.2 M GdmCl to final GdmCl concentrations ranging from 0.2 to 1.8 M. Unfolding experiments used 1:1 ratio mixing sizes such that 1 part native IL-1β dilutes into 1 part GdmCl buffer. Excitation was at 293 nm, and emission was collected through a >320 nm cutoff filter. Each kinetic trace is the average of 10−20 data acquisitions.

Data Analysis. The total fluorescence emission I_{total} was determined by the sum of the intensity between 300 and 450 nm as given in eq 1:

$$I_{total} = \sum_{300-450nm} I_\lambda \tag{1}$$

It should be noted that that quantitative titration measurements of chemical reactions using I_{total} as a probe can be complicated by the fact that different absorbance extinction coefficients between the reactant and product will give inaccurate results (*17*). Fortunately, the extinction coefficients between native ($\epsilon_{280} = 11.26\ mM^{-1}\ cm^{-1}$) and unfolded ($\epsilon_{280} = 11.10\ mM^{-1}\ cm^{-1}$) states of IL-1$\beta$ are very similar and allow the use of tryptophan fluorescence for quantitative folding measurements (*17*).

The average fluorescence wavelength $\lambda_{average}$ was determined by the center of mass of the fluorescence spectra given in eq 2:

$$\lambda_{average} = \frac{\sum_{300-450nm} \lambda * I_\lambda}{\sum_{300-450nm} \lambda} \tag{2}$$

where λ is the wavelength of light in nanometers at each point in the spectra and I_λ is the intensity of light at wavelength λ. It should be noted that quantitative titration measurements of chemical reactions using $\lambda_{average}$ as a probe can be complicated by the fact that different fluorescence intensities (I_{total}) between the reactant and product will give inaccurate results (*17*). Since this is the case with IL-1β native and unfolded states, $\lambda_{average}$ should be used only as a qualitative probe.

Equilibrium fluorescence data were fit with in-house software a two state model:

$$X \rightleftarrows U \tag{3}$$

where the protein can either be in a folded state, X, or the unfolded state, U (*18*). This analysis may be applied to any experimentally detectable folding species, such as X = N, the stable native state or X = I, a metastable kinetic folding intermediate (*18*). The apparent fraction of unfolded state, F_{XU}^{app}, populated at given GdmCl concentration [GdmCl] is estimated from the observed signal $S^{observed}$, the linear extrapolation of the [GdmCl]-dependent baseline signal of the species X ($S_X^{[GdmCl]=0} + S'_X[GdmCl]$), and the linear extrapolation of the [GdmCl] dependent baseline signal of the unfolded ensemble U ($S_U^{[GdmCl]=0} + S'_U[GdmCl]$) with eq 4a:

$$F_{XU}^{app} = \frac{S^{observed} - (S_X^{[GdmCl]=0} + S'_X[GdmCl])}{(S_U^{[GdmCl]=0} + S'_U[GdmCl]) - (S_X^{[GdmCl]=0} + S'_X[GdmCl])} \tag{4a}$$

The apparent free energy of unfolding species X, ΔG_{XU}^{app}, is fit from the estimated values of F_{XU}^{app} with eq 4b:

$$F_{XU}^{app} = \frac{e^{-\Delta G_{XU}^{app}/RT}}{1 + e^{-\Delta G_{XU}^{app}/RT}} \quad (4b)$$

The free energy of unfolding species X at 0 M GdmCl, $\Delta G_{XU}^{H_2O}$, is determined by extrapolating ΔG_{XU}^{app} to 0 M GdmCl with a linear free energy dependence term, m_{XU}, and is shown in eq 5 (*19*, *20*):

$$\Delta G_{XU}^{app} = \Delta\Delta G_{XU}^{H_2O} + m_{XU}[\text{GdmCl}] \quad (5)$$

Manual mixing and stopped flow kinetic data were fit to eq 6 using the Marquardt algorithm (*21*) and in-house software

$$A(t) = \sum_{i=1}^{n} A_i e^{-\lambda_i t} + A(\infty) \quad (6)$$

The number of kinetic processes *i*, observed rate constant λ_i, signal amplitude A_i of each exponential kinetic process *i* and the final signal value $A(8)$ at equilibrium were determined using the fit quality represented in the reduced chi-squared (χ_r^2) values (*22*), the random dispersion of residuals, and the logical consistency of the generated fitting parameters. The observed rate constants, λ_i, do not necessarily measure the true microscopic rate constant k_i for a kinetic process (*23*, *24*).

RESULTS

Equilibrium Fluorescence pH Tirations. Figure 1A shows the effect of pH on the total fluorescence emission I_{total} of native and unfolded IL-1β. The I_{total} of native IL-1β increases from 2.45×10^9 cps to 1.65×10^9 cps as the pH is lowered from 7 to 5. The I_{total} of the unfolded ensemble remains relatively constant at 1.65×10^9 cps and is insensitive to changes in solution pH. Figure 1B shows the effect of pH on the average fluorescent wavelength, $\lambda_{average}$, of native and unfolded IL-1β. The $\lambda_{average}$ is 345 nm for native IL-1β and 353 nm for unfolded IL-1β. Neither native nor unfolded $\lambda_{average}$ is altered by a pH change between 5 and 7.

Equilibrium Fluorescence GdmCl Tirations. Equilibrium total fluorescence emission during GdmCl titration of IL-1β at pH 5.0, 5.3, 5.8, 6.0, 6.2, 6.3, 6.5, and 7.0 are shown in Figure 2A. The center of the transition region is at a higher GdmCl concentration at lower pH, indicating an increase in stability at lower pH. This apparent increase in stability is confirmed by fitting the equilibrium transitions in Figure 2A for thermodynamic stability $\Delta G_{NU}^{H_2O}$ (kcal/mol) and GdmCl sensitivity m_{NU} (kcal mol^{-1} [GdmCl]$^{-1}$) using eqs 4a, 4b, and 5 (see Methods). Figure 2B shows the fitted values for the thermodynamic stability $\Delta G_{NU}^{H_2O}$ (kcal/mol) and GdmCl sensitivity m_{NU} (kcal mol^{-1} [GdmCl]$^{-1}$) at pH 5.0, 5.3, 5.8, 6.0, 6.2, 6.3, 6.5, and 7.0. The GdmCl sensitivity m_{NU} is 5.1 $\pm$ 0.40 kcal mol^{-1} [GdmCl]$^{-1}$ and insensitive to changes in solution pH. Since m_{NU} has been shown to be independent of pH, the reported error is determined at the 95% confidence interval using a value of m_{NU} measured at each of the eight pH conditions (8 independent measurements of m_{NU}/7 degrees of freedom). The thermodynamic stability

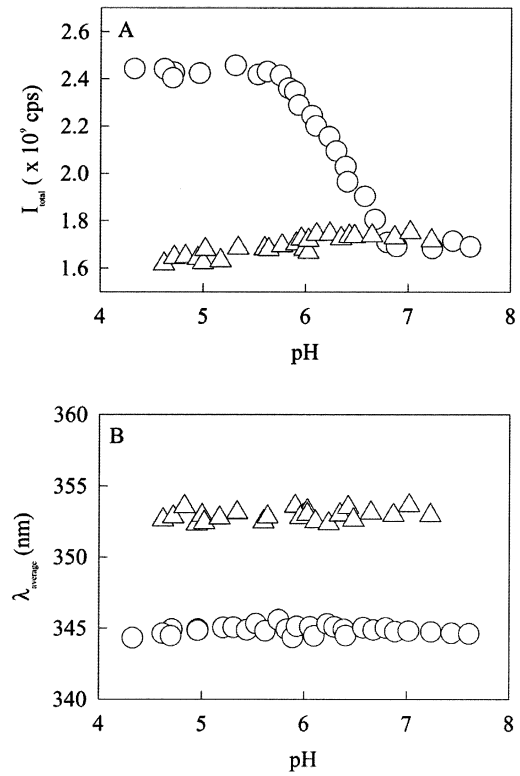

FIGURE 1: (A) Tryptophan fluorescence emission (I_{total}) of native IL-1β (○) and IL-1β unfolded in 3M GdmCl (△) at pH between 5 and 7. (B) Average fluorescence wavelength ($\lambda_{average}$) of native IL-1β (○) and IL-1β unfolded in 3M GdmCl (△) at pH between 5 and 7.

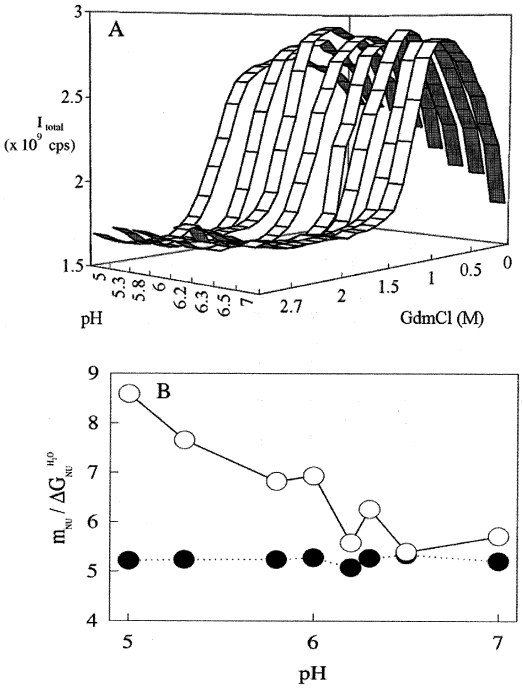

FIGURE 2: (A) Tryptophan fluorescence emission (I_{total}) from GdmCl titrations of IL-1β at pH between 5 and 7. (B) Parameters $\Delta G_{NU}^{H_2O}$ (—○—) and *m*-value m_{NU} (--●--) fit using eqs 4a, 4b, and 5 for each GdmCl titration between pH 5 and 7.

$\Delta G_{NU}^{H_2O}$ decreases from 8.5 to 5.5 kcal/mol as pH is increased from 5 to 7.

Fluorescence Measured Kinetics. A plot of the change in fluorescence intensity as a function of time for a stopped-

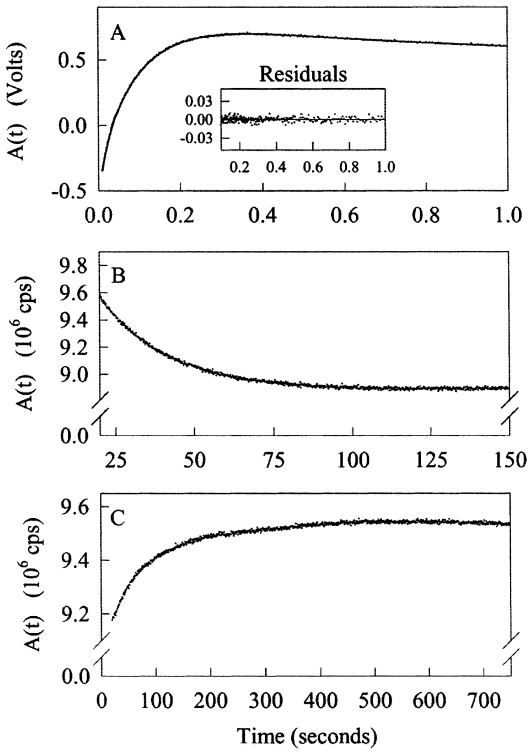

FIGURE 3: Real-time kinetic fluorescence measurements during the refolding of IL-1β at pH 5. (A) Refolding from 2.2 to 0.2 M GdmCl at pH 5.0 by stopped flow mixing. Individual data points are shown along with a 2-exponential fit (—). (inset) Residuals of the kinetics fit to two exponential processes, λ_2 and λ_1. (B) Refolding from 2.2 to 0.2 M GdmCl at pH 5.0 by manual mixing. Under these conditions, the displayed process λ_1 is characterized by a decrease in fluorescence with time. (C) Refolding from 2.2 to 1.0 M GdmCl at pH 5.0 by manual mixing. Under these conditions, the displayed process λ_1 is characterized by an increase in fluorescence with time.

flow refolding jump of WT IL-1β from 2.2 to 0.2 M GdmCl at pH 5.0 is given in Figure 3A. The first 1 s of the reaction is shown for clarity. An initial increase in fluorescence intensity followed by a slower decay to the expected equilibrium value and fits to two exponential processes with observed rate constants λ_2 (fast) and λ_1 (slow). The observed rate constant of fluorescence increase, λ_2, measures the population of a highly fluorescent intermediate from the unfolded state. The subsequent observed rate constant of fluorescence decrease, λ_1, measures the population of the native state from the intermediate. This model of IL-1β folding from fluorescence data is consistent with species detected using pulse-labeling techniques (*3*, *5*). The calculated fit of the data to two exponential process is shown for comparison (Figure 3A). The plot of the residual errors for the fit of the data to a two exponential equation is given in the inset to Figure 3A. As demonstrated in Figure 3B (0.2 M GdmCl) and 3C (1.0 M GdmCl), the slower process λ_1 has either a negative (Figure 3B) or positive (Figure 3C) fluorescence amplitude, depending upon the final GdmCl concentration in the refolding jumps as described in previous work (*4*, *25*). This observation is consistent with the changes in equilibrium fluorescence measurements of the native state observed between 0.2 and 1.0 M GdmCl, respectively. Analysis of both WT and K97I unfolding fluorescence data under all conditions fit best to one exponential process, the observed rate constant consistent with λ_1. The faster observed rate process, λ_2, is observed in refolding but not observed in

Scheme 1

unfolding experiments by either manual mixing or stopped flow techniques (data not shown). At high GdmCl concentrations, the intermediate is not significantly populated and thus observed rate constant λ_1 measures the transition from the native to the unfolded state. Furthermore, the rate of the λ_2 transition is significantly faster than λ_1. In unfolding experiments of IL-1β, the slower process λ_1 precedes the faster process λ_2 and would therefore "mask" the λ_2 amplitude, such that only λ_1 would be effectively observed. However, it should be noted that values of λ_2 under unfolding conditions can be estimated from refolding measurements in the transition region (1.4−2.0 M [GdmCl]).

Fluorescence-detected folding kinetics for IL-1β were performed over a series of final GdmCl and pH concentrations. Previous experiments have shown that the IL-1β folding kinetics, in the absence of aggregation, can be adequately characterized with a two exponential fit (*4*, *26*). Taken together with hydrogen−deuterium exchange pulse labeling studies (*5*), these kinetics have been shown to fit best to a sequential, on-pathway, folding mechanism with three observed folding states (U, I, N) and two measurable transition states (T_2, T_1), shown in Scheme 1.

In a kinetic model of Scheme 1, the measured values of observed rates λ_2 and λ_1, are determined using the following relationships between the macroscopic rate constants for refolding, k_{UT_2} and k_{IT_1}, and unfolding, k_{IT_2} and k_{NT_1} (*23*, *24*):

$$\lambda_2 = k_{UT_2} + \left[\frac{k_{NT_1}}{k_{IT_1} + k_{NT_1}}\right] * k_{IT_2} \quad (7)$$

$$\lambda_1 = \left[\frac{k_{UT_2}}{k_{UT_2} + k_{IT_2}}\right] * k_{IT_1} + k_{NT_1} \quad (8)$$

At low [GdmCl] (≤0.8 M), refolding rate constants are much greater than unfolding rate constants ($k_{UT_2} \gg k_{IT_2}$; $k_{IT_1} \gg k_{NT_1}$), and the parameters λ_2 and λ_1 can be approximated with eqs 9ab and 10ab:

$$\lambda_2 = k_{UT_2} \quad (9a)$$

$$= k_{UT_1}^{H_2O} e^{m_{UT2}[GdmCl]/RT} \quad (9b)$$

$$\lambda_1 = k_{IT_1} \quad (10a)$$

$$= k_{IT_1}^{H_2O} e^{m_{IT1}[GdmCl]/RT} \quad (10b)$$

In eq 9b, $k_{UT_2}^{H_2O}$ is the value of rate constant k_{UT_2} extrapolated to 0 M GdmCl and multiplication of $k_{UT_2}^{H_2O}$ by the term $e^{m_{UT2}[GdmCl]/RT}$ determines the rate constant k_{UT_2} at a given [GdmCl] concentration. In eq 10b, $k_{IT_1}^{H_2O}$ is the value of k_{IT_1} extrapolated to 0 M GdmCl and multiplication of $k_{IT_1}^{H_2O}$ by the term $e^{mm_{IT1}[GdmCl]/RT}$ determines the rate constant k_{IT_1} at a given [GdmCl] concentration.

Under refolding conditions (≤0.8 M GdmCl), a linear estimation model can be used to determine refolding free

energy barriers from the observed rates, λ_2 and λ_1, at varying GdmCl concentrations using eqs 11ab and 12ab (*19*, *20*):

$$\Delta G^{app}_{UT_2} = -RT \ln\left(\frac{\lambda_2 h}{k_B T}\right) \quad (11a)$$

$$= \Delta G^{H_2O}_{UT_2} + m_{UT_2}[GdmCl] \quad (11b)$$

$$\Delta G^{app}_{IT_1} = -RT \ln\left(\frac{\lambda_1 h}{k_B T}\right) \quad (12a)$$

$$= \Delta G^{H_2O}_{IT_1} + m_{IT_1}[GdmCl] \quad (12b)$$

At higher [GdmCl] ($\geq$1.4 M), unfolding rate constants are much greater than refolding rate constants ($k_{IT_2} \gg k_{UT_2}$; $k_{NT_1} \gg k_{IT_1}$) and the parameters λ_2 and λ_1 can be approximated with eqs 13ab and 14ab:

$$\lambda_2 = k_{IT_2} \quad (13a)$$

$$= k^{H_2O}_{IT_2} e^{m_{IT2}[GdmCl]/RT} \quad (13b)$$

$$\lambda_1 = k_{NT_1} \quad (14a)$$

$$= k^{H_2O}_{NT_1} e^{m_{NT1}[GdmCl]/RT} \quad (14b)$$

In eq 13b, $k^{H_2O}_{IT_2}$ is the value of k_{IT_2} extrapolated to 0 M GdmCl and multiplication of $k^{H_2O}_{IT_2}$ by the term $e^{m_{IT2}[GdmCl]/RT}$ determines the rate constant k_{IT_2} at a given [GdmCl] concentration. In eq 14b, $k^{H_2O}_{NT_1}$ is the value of k_{NT_1} extrapolated to 0 M GdmCl and multiplication of $k^{H_2O}_{NT_1}$ by the term $e^{m_{NT1}[GdmCl]/RT}$ determines the rate constant k_{NT_1} at a given [GdmCl] concentration.

Under unfolding conditions ($\geq$1.4 M GdmCl), a linear estimation model can be used to determine unfolding free energy barriers from observed rates, λ_2 and λ_1, using eqs 15ab and 16ab (*19*, *20*):

$$\Delta G^{app}_{IT_2} = -RT \ln\left(\frac{\lambda_2 h}{k_B T}\right) \quad (15a)$$

$$= \Delta G^{H_2O}_{IT_2} + m_{IT_2}[GdmCl] \quad (15b)$$

$$\Delta k^{app}_{NT_1} = -RT \ln\left(\frac{\lambda_1 h}{k_B T}\right) \quad (16a)$$

$$= \Delta G^{H_2O}_{NT_1} + m_{NT_1}[GdmCl] \quad (16b)$$

The use of k_BT/h as a preexponential factor in eqs 11a, 12a, 15a, and 16a is a subject of considerable debate as the value of $k_BT/h = 10^{-12}$ is the preexponential factor for a single bond vibration (*27*). Although it has often been used to estimate the free energy of folding barriers, other studies have used a lower value, such as a diffusion-limited preexponential factor 10^{-10}, based on the fact that protein folding is clearly a more complex process than a single bond vibration (*28*). However, this study focuses on the change in the transition state free energy through the perturbation by GdmCl and pH, in which a free energy change is the important value and the absolute free energy values are of lesser importance. In other words, as long as the preexponential term remains constant over the range of pH and GdmCl concentrations studied, using eqs 11ab, 12ab, 15ab, and 16ab is appropriate in the analysis of protein folding.

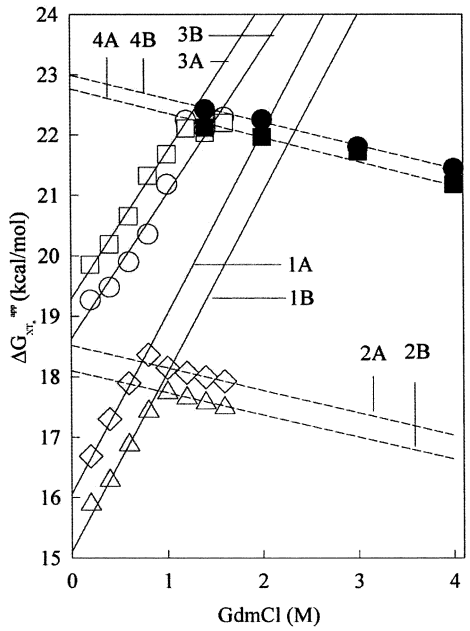

FIGURE 4: Free energy barriers, $\Delta G^{app}_{XT_n}$, of the transition states calculated from observed kinetic processes, λ_2 and λ_1. Free energy barrier $\Delta G^{app}_{XT_n}$, determined from λ_2 by stopped-flow refolding, is shown at pH 5.0 (△) and 7.0 (◇). Free energy barrier $\Delta G^{app}_{XT_n}$, determined from λ_1 by manual-mixing refolding, is shown at pH 5.0 (○) and 7.0 (□). Free energy barrier $\Delta G^{app}_{XT_n}$, determined from λ_1 by manual-mixing unfolding, is shown at pH 5.0 (●) and 7.0 (■). Fits of the microscopic energy barriers $\Delta G^{app}_{UT_2}$ at pH 7 (Label 1A), $\Delta G^{app}_{UT_2}$ at pH 5 (Label 1B), $\Delta G^{app}_{IT_2}$ at pH 7 (Label 2A), $\Delta G^{app}_{IT_2}$ at pH 5 (Label 2B), $\Delta G^{app}_{IT_2}$ at pH 7 (Label 3A), $\Delta G^{app}_{IT_2}$ at pH 5 (Label 3B), $\Delta G^{app}_{NT_1}$ at pH 7 (Label 4A), and $\Delta G^{app}_{NT_1}$ at pH 5 (Label 4B).

Figure 4 shows the apparent transition state free energy barrier, $\Delta G^{app}_{XT_n}$, between a populated folding species (X) and a neighboring transition state (T_n). Barrier values of $\Delta G^{app}_{XT_n}$, calculated using eqs 11a/15a for the λ_2 transition and 12a/16a for the λ_1 transition, are displayed in a typical "chevron plot" over a range of GdmCl concentrations. It is important to note that, even though the λ_2 transition is not observed in unfolding experiments, refolding measurements of λ_2 in the transition region (1.4−2.0 M [GdmCl]) can be used to estimate $\Delta G^{app}_{IT_2}$ via eq 15b. The energy barriers for folding kinetics are shown at pH 5 and 7 to indicate the effect of pH on $\Delta G^{app}_{XT_n}$ values.

The assumption of linear free energy barrier change with [GdmCl], shown in eqs 11b, 12b, 15b, and 16b, is confirmed in Figure 4 by the expected "chevron" shape of $\Delta G^{app}_{XT_n}$ observed between 0 and 4 M GdmCl. $\Delta G^{app}_{XT_n}$ calculated from λ_2 and λ_1 increase linearly between 0 and 0.8 M GdmCl, confirming that eqs 11b and 12b apply at GdmCl concentrations $\leq$0.8 M. $\Delta G^{app}_{XT_n}$ calculated from λ_2 and λ_1 decrease linearly between 1.4 and 4.0 M GdmCl, confirming that eqs 15b and 16b apply at GdmCl concentrations $\geq$1.4 M.

Also shown in Figure 4 are fits of eqs 11b, 12b, 15b, and 16b to the apparent transition state free energy barriers at varying GdmCl concentrations. Fits of $\Delta G^{app}_{XT_n}$ values to eqs 11b, 12b, 15b, and 16b are shown at pH 5 and 7 to show

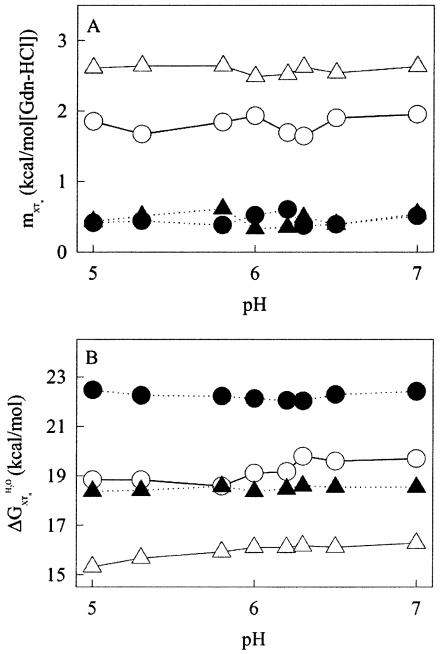

FIGURE 5: (A) Fitted *m*-values m_{UT_2} (−△−), m_{IT_1} (−○−), m_{IT_2} (--▲--), and m_{NT_1} (--●--). (B) Fitted microscopic free energy barriers extrapolated to 0 M GdmCl: $\Delta G^{H_2O}_{UT_2}$ (−△−), $\Delta G^{H_2O}_{IT_1}$ (−○−), $\Delta G^{H_2O}_{IT_2}$ (--▲--), and $\Delta G^{H_2O}_{NT_1}$ (--●--).

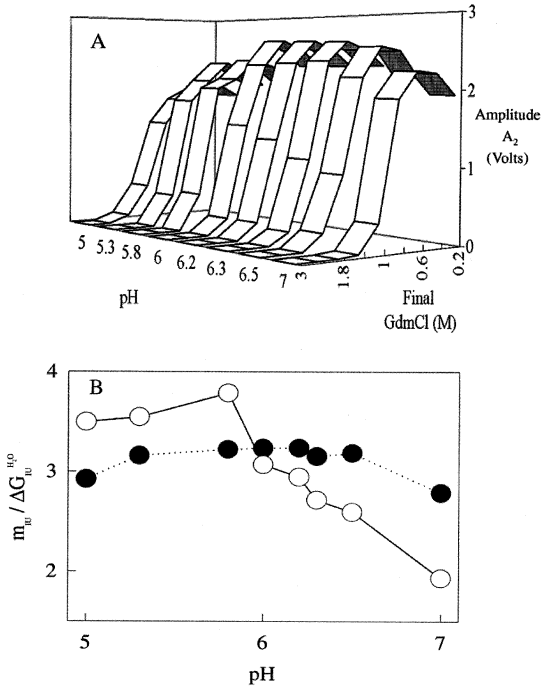

FIGURE 6: (A) IL-1β tryptophan emission amplitude, A_2, of the λ_2 refolding process measured with stopped flow fluorescence at increasing GdmCl concentrations and at varying pH between 5 and 7. (B) Parameters $\Delta G^{H_2O}_{IU}$ (−○−) and *m*-value m_{IU} (--●--), fit using λ_2 amplitudes in eqs 4a, 4b, and 5 for each GdmCl titration between pH 5 and 7.

the effect of pH on IL-1β folding kinetics. Refolding transition states $\Delta G^{app}_{UT_2}$ and $\Delta G^{app}_{IT_1}$ are fit at GdmCl concentrations ≤0.8 M, where eqs 11b and 12b are applicable. Unfolding transition states $\Delta G^{app}_{IT_2}$ and $\Delta G^{app}_{NT_1}$ are fit at GdmCl concentrations ≥1.4 M, where eqs 15b and 16b are applicable.

Kinetic parameters, $\Delta k^{H_2O}_{XT_n}$ and m_{XT_n}, are fit from eqs 11b, 12b, 15b, and 16b between pH 5−7 and are shown in Figure 5. Figure 5A shows refolding and unfolding transition state *m*-values m_{XT_n} are not altered by pH changes between 5 and 7. For refolding, $m_{UT_2} = 2.6 \pm 0.32$ kcal mol^{-1} [GdmCl]$^{-1}$ and $m_{IT_1} = 1.8 \pm 0.66$ kcal mol^{-1} [GdmCl]$^{-1}$. For unfolding, $m_{IT_2} = 0.46 \pm 0.52$ kcal mol^{-1} [GdmCl]$^{-1}$ and $m_{NT_1} = 0.45 \pm 0.44$ kcal mol^{-1} [GdmCl]$^{-1}$. Since all values of m_{XT_n} are observed to be independent of pH, the reported error is determined at the 95% confidence interval using a value of m_{UT_2}, m_{IT_1}, m_{IT_2}, and m_{NT_1} measured at each of the eight pH conditions (8 independent measurements of m_{UT_2}, m_{IT_1}, m_{IT_2}, and m_{NT_1}/7 degrees of freedom). It must be noted that values of m_{IT_2} and m_{NT_1} for unfolding transitions are on the threshold of statistical significance since their overall values are quite similar to the 95% confidence error of repeated manual-mixing kinetic measurements. Thus, while it is statistically significant that the values of m_{IT_2} and m_{NT_1} are small (<1 kcal mol^{-1} [GdmCl]$^{-1}$), it cannot be determined with greater than 95% confidence that their values are not actually zero (i.e., they reject the null hypothesis).

Figure 5B shows transition state energies extrapolated to zero [GdmCl], $\Delta G^{H_2O}_{XT_n}$, between pH 5 and 7. $\Delta G^{H_2O}_{UT_2}$ increases from 15.1 to 16.6 kcal/mol as pH is increased from 5 to 7, indicating that the refolding U → T_2 transition barrier is affected by pH changes. $\Delta G^{H_2O}_{IT_1}$ increases from 18.3 to 20.3 kcal/mol as pH is increased from 5 to 7, indicating that the I → T_1 refolding transition barrier is also affected by pH changes. $\Delta G^{H_2O}_{IT_2}$ and $\Delta G^{H_2O}_{NT_1}$ remain unchanged at 18.5 ± 0.48 and 22.2 ± 0.84 kcal/mol, respectively, as pH is increased from 5 to 7, indicating that the unfolding I → T_2 and N → T_1 transition barriers are unaffected by pH changes in this range. Since unfolding transition barriers, $\Delta G^{H_2O}_{IT_2}$ and $\Delta G^{H_2O}_{NT_1}$ are observed to be independent of pH, the reported error is determined at the 95% confidence interval using a value of $\Delta G^{H_2O}_{IT_2}$ or $\Delta G^{H_2O}_{NT_1}$ measured at each of the eight pH conditions (8 independent measurements of $\Delta G^{H_2O}_{IT_2}$ or $\Delta G^{H_2O}_{NT_1}$/7 degrees of freedom).

Amplitude Analysis. A global fit of IL-1β kinetic amplitudes is not as informative as the change in sign of the fluorescence signal for the λ_1 refolding amplitude, A_1, between low and high GdmCl concentrations, as described previously (Figure 3B,C) (*4*). However, the λ_2 amplitude, A_2, is positive at all GdmCl concentrations and can be used to estimate the thermodynamic stability $\Delta G^{H_2O}_{IU}$ and *m*-value m_{IU} for the kinetic intermediate I (*18*). Figure 6A shows A_2 between 0 and 3 M GdmCl and pH 5−7. In Figure 6A, the GdmCl concentration of the transition midpoint C_M is shown to shift to higher GdmCl concentrations as pH changes from 7 to 5. Figure 6B shows the parameters $\Delta G^{H_2O}_{IU}$ and m_{IU} between pH 5−7, fitted from eqs 4a, 4b, and 5 using the measured amplitude $A_2 = S^{observed}$ in eq 4a. Parameter $m_{IU} = 3.1 \pm 0.88$ kcal mol^{-1} [GdmCl]$^{-1}$ and is largely unchanged between pH 5−7. Since the value of m_{IU} is observed to be independent of pH, the reported error is determined at the 95% confidence interval using a value of m_{IU} measured at each of the eight pH conditions (8 independent measurements of m_{IU}/7 degrees of freedom). However, the parameter $\Delta G^{H_2O}_{IU}$ does change with pH. $\Delta G^{H_2O}_{IU}$ decreases from 3.5 kcal/mol at pH 5 to 2.0 kcal/mol at pH 7. This trend of

decreasing intermediate stability, $\Delta G_{IU}^{H_2O}$, is similar to the decreasing native state stability, $\Delta G_{NU}^{H_2O}$, from pH 5−7.

DISCUSSION

Native IL-1β Undergoes Stability Changes between pH 5 and 7. It is evident from Figure 1A that the tryptophan 120 fluorescence emission is quenched as pH is increased from 5 to 7. However, as shown qualitatively in Figure 1B, this pH change does not alter the average fluorescent wavelength and therefore does not significantly alter the solvent accessibility of Trp120. The results of Figure 1A and 1B are consistent with an earlier biophysical study (*1*). The secondary structure difference between IL-1β at pH 5.4 and 7 shows little difference, and the observed fluorescence emission change is proposed to result from local structural and/or electrostatic changes near Trp120 (*29*).

To determine whether the fluorescence changes in Figure 1A correlate with changes in thermodynamic stability, GdmCl titrations of IL-1β were performed at various solution pH values (Figure 2A). In Figure 2B, it is shown that thermodynamic stability $\Delta G_{NU}^{H_2O}$ decreases from 8.5 to 5.2 kcal/mol as pH is increased from 5 to 7. The *m*-value m_{NU} is 5.1 ± 0.4 and is not significantly affected between pH 5−7. The values of $\Delta G_{NU}^{H_2O}$ and m_{NU} are in good agreement with $\Delta G_{NU}^{H_2O}$ and m_{NU} values measured in previous experiments (*1*, *30*). Small deviations between the parameters reported in the present study and previously reported experimental values may be due to different buffer conditions or fitting methods (*31*).

The *m*-value has been shown to correlate linearly with the amount of solvent accessible surface area difference between an unfolded polypeptide chain and native state (ΔSASA) in a number of proteins (*7*). Thus, the absence of pH-dependent changes in GdmCl sensitivity m_{NU} (Figure 2A) and the average fluorescent wavelength $\lambda_{average}$ (Figure 1B) suggest that the amount of surface area buried by native IL-1β does not change significantly between pH 5 and 7.

Refolding IL-1β Transition State Stabilities Change between pH 5 and 7. Two refolding transitions and two unfolding transitions can be accurately measured with kinetic measurements of IL-1β folding (Figure 3). It is important to note that the observed rate of the unfolding transition I → U can only be quantitated from refolding experiments in the transition region (1.4−2.0 M GdmCl) and is not observed in unfolding experiments (see Results). The *m*-values of the folding transitions, T_2 and T_1, remain unchanged between pH 5 and 7 (Figure 5A). In addition, refolding *m*-values, m_{UT_2} and m_{IT_1}, are significantly larger than unfolding *m*-values, m_{IT_2} and m_{NT_1}. Figure 5B shows that $\Delta G_{XN_2}^{H_2O}$ values are changed by pH. These changes are most evident in refolding parameters, $\Delta G_{UT_2}^{H_2O}$ and $\Delta G_{IT_2}^{H_2O}$, and are not significantly observed in the unfolding parameters, $\Delta G_{IT_2}^{H_2O}$ and $\Delta G_{NT_1}^{H_2O}$. Thus, the native state stability $\Delta G_{NU}^{H_2O}$ decrease (Figure 2B) corresponds with increases in the refolding, not unfolding, transition state energy barriers, $\Delta G_{UT_2}^{H_2O}$ and $\Delta G_{IT_1}^{H_2O}$ (Figure 5B), as the pH is increased from 5 to 7.

The Thermodynamics of IL-1β Folded States Can Be Accurately Described with a Sequential Three-State Kinetic Model. Figure 6A,B shows that the IL-1β kinetic intermediate stability $\Delta G_{IU}^{H_2O}$, but not *m*-value m_{IU}, decreases as pH is shifted from 5 to 7. The trends in these parameters are similar to those of the native state parameters $\Delta G_{NU}^{H_2O}$ and m_{NU}, indicating similar structural properties between the intermediate and native state. This finding is consistent with a sequential IL-1β folding mechanism and an on-pathway intermediate (*5*). However, at present, a full assessment of whether the kinetic parameters of whether this sequential three-state kinetic model is in agreement with the thermodynamic parameters of the stable native state and the metastable intermediate ensemble has yet to be done.

An initial test of any kinetic folding model is whether it can reproduce the native state thermodynamic parameters determined from equilibrium studies ($\Delta G_{NU}^{H_2O}$ and m_{NU}) (Figure 2A,B) using parameters measured from kinetic rates. Also, thermodynamic analysis of the λ_2 kinetic amplitude A_2 has been used to measure the thermodynamic parameters of the intermediate species ($\Delta G_{IU}^{H_2O}$ and m_{IU}) (Figure 6A,B), which are also important values to compare with the proposed kinetic model.

To compare a proposed kinetic model with preexisting thermodynamic data, parameters obtained from kinetic studies must be converted into thermodynamic values. For a simple sequential mechanism, the thermodynamic value of any species along the folding pathway is obtained through direct summation of the kinetic transition state parameters, $\Delta G_{XT_n}^{H_2O}$ and m_{XT_n}, up to that species (*32*). It is important to note that, for determination of free energies by this method, summation of the refolding free energy barrier heights is additive while the barrier heights of unfolding transitions are subtracted from the total. Thus, to accept the three-state sequential folding model in Scheme 1 as a valid model, a number of comparisons must be made.

First, the sum of kinetic *m*-values, $m_{IU}^{kinetic} = m_{UT_2} + m_{IT_2}$, should be roughly equivalent to the equilibrium intermediate *m*-value, m_{IU} (determined from kinetic amplitude analysis in Figures 6AB)

$$m_{IU} \approx m_{IU}^{kinetic} = m_{UT_2} + m_{IT_2} \quad (17)$$

Second, the sum of kinetic *m*-values, $m_{NU}^{kinetic} = m_{UT_2} + m_{IT_2} + m_{IT_1} + m_{NT_1}$, should be roughly equivalent to the equilibrium native *m*-value, m_{NU} (determined from equilibrium GdmCl titration in Figures 2AB)

$$m_{NU} \approx m_{NU}^{kinetic} = m_{UT_2} + m_{IT_2} + m_{IT_1} + m_{NT_1} \quad (18)$$

Third, the sum of kinetic Δ*G*-values, $\Delta G_{IU}^{kinetic} = \Delta G_{UT_2}^{H_2O} - \Delta G_{IT_2}^{H_2O}$, should be roughly equivalent to the equilibrium intermediate Δ*G*-value, $\Delta G_{IU}^{H_2O}$ (determined from kinetic amplitude analysis in Figures 6AB)

$$\Delta G_{IU}^{H_2O} \approx \Delta G_{IU}^{kinetic} = \Delta G_{UT_2}^{H_2O} - \Delta G_{IT_2}^{H_2O} \quad (19)$$

Last, the sum of kinetic Δ*G*-values, $\Delta G_{NU}^{kinetic} = \Delta G_{UT_2}^{H_2O} - \Delta G_{IT_2}^{H_2O} + \Delta G_{IT_1}^{H_2O} - \Delta G_{NT_1}^{H_2O}$, should be roughly equivalent to the equilibrium native ΔG-value, $\Delta G_{NU}^{H_2O}$ (determined from equilibrium GdmCl titration in Figures 2AB)

$$\Delta G_{NU}^{H_2O} \approx \Delta G_{NU}^{kinetic} = \Delta G_{UT_2}^{H_2O} - \Delta G_{IT_2}^{H_2O} + \Delta G_{IT_1}^{H_2O} - \Delta G_{NT_1}^{H_2O} \quad (20)$$

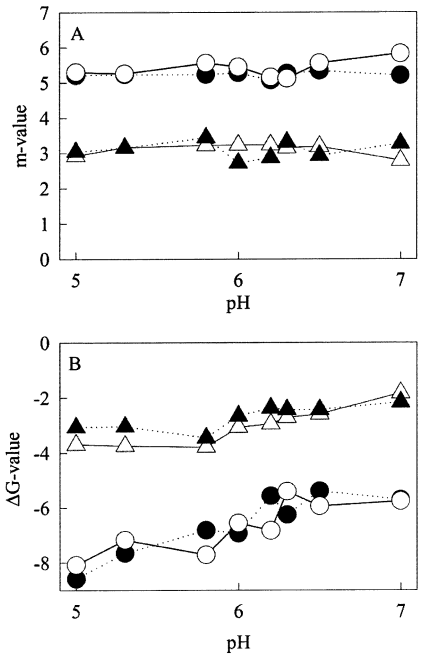

FIGURE 7: (A) Comparison of the *m*-values obtained by kinetic and equilibrium methods. Comparison of the *m*-values for the IL-1β intermediate I measured by kinetic methods, $m_{IU}^{kinetic}$ (--▲--), and equilibrium methods, m_{IU} (−△−). Comparison of the *m*-values for the IL-1β native state N measured by kinetic methods, $m_{NU}^{kinetic}$ (--●--), and equilibrium methods, m_{NU} (−○−). (B) Comparison of the ΔG-values obtained by kinetic and equilibrium methods. Comparison of the ΔG-values for the IL-1β intermediate I measured by kinetic methods, $\Delta G_{IU}^{kinetic}$ (--▲--), and equilibrium methods, $\Delta G_{IU}^{H_2O}$ (−△−). Comparison of the *m*-values for the IL-1β native state N measured by kinetic methods, $\Delta G_{NU}^{kinetic}$ (--●--), and equilibrium methods, $\Delta G_{NU}^{H_2O}$ (−○−).

Figure 7AB indicates that the agreement between kinetic and equilibrium parameters shown in eqs 17−20 does indeed exist in the pH range 5−7. Figure 7A shows that the kinetic *m*-value calculations, $m_{IU}^{kinetic} = 3.1 \pm 1.3$ kcal mol^{-1} [GdmCl]$^{-1}$ and $m_{NU}^{kinetic} = 5.4 \pm 1.3$ kcal mol^{-1} [GdmCl]$^{-1}$, are roughly equivalent to the equilibrium *m*-value measurements, $m_{IU} = 3.1 \pm 0.88$ kcal mol^{-1} [GdmCl]$^{-1}$ and $m_{NU} = 5.2 \pm 0.40$ kcal mol^{-1} [GdmCl]$^{-1}$, respectively, in the pH range 5−7. Since both kinetic and equilibrium *m*-values are observed to be independent of pH, the reported error is determined at the 95% confidence interval using the *m*-values measured at each of the eight pH conditions (8 independent *m*-value measurements/7 degrees of freedom).

Figure 7B shows that the kinetic ΔG-value calculations, $\Delta G_{IU}^{kinetic}$ and $\Delta G_{NU}^{kinetic}$, are roughly equivalent to the equilibrium ΔG-value measurements, $\Delta G_{IU}^{H_2O}$ and $\Delta G_{NU}^{H_2O}$, respectively, in the pH range 5−7. This observed agreement between equilibrium measurements and kinetic measurements of IL-1β folding parameters provides strong evidence supporting the three-state sequential mechanism proposed in Scheme 1. Any additional macroscopic folding species, if present, would contribute a minimal contribution to free energy or solvent accessibility changes beyond that of U, I, and N.

The *m*-values in Figure 5A and ΔG-values in Figure 5B can be represented in a free energy diagram of IL-1β folding in accordance with the sequential mechanism of Scheme 1 (Figure 8). Shown in Figure 8 is the free energy profile of

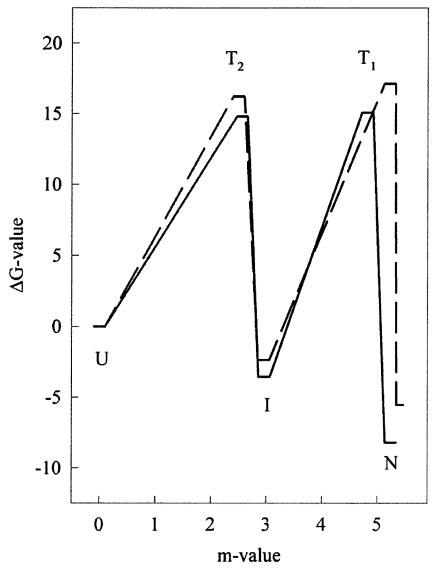

FIGURE 8: Free energy profile of the IL-1β folding reaction, plotting the free energy ΔG-values vs *m*-values of unfolded ensemble (U), U ⇄ I transition state (T_2), intermediate (I), I ⇄ N transition state (T_1), and native (N) folding species. Also shown for comparison is the free energy profile of IL-1β at pH 5 (—) and pH 7 (---). The *x*-axis reaction coordinate is characterized by the summation of *m*-values and is assumed to be proportional to the fraction of native solvent accessible surface area buried in each species.

sequential IL-1β folding in Scheme 1 between unfolded ensemble U, U → I transition state T_2, intermediate I, I → N transition state T_1, and native state N. It should be noted that the mechanism shown in Figure 8 is based on two simplifying assumptions. The first assumption is that, as mentioned earlier (see Results), the transition state free energy barrier heights have been quantitated using h/k_BT as the preexponential factor. The second assumption is that IL-1β folding occurs through a single pathway occupied by discrete states U, T_1, I, T_2, and N when, in fact, these macroscopic states are each an ensemble of microscopic states. This second assumption can be justified by the fact that simplified pathways, such as that shown in Figure 8, can successfully characterize macroscopic protein folding experiments which measure the average properties of the protein ensemble (*27*). Furthermore, limitations of macroscopic experimental data preclude fitting protein folding measurements with overly complex microscopic models. To address these assumptions in the future, work on IL-1β folding will be directed at quantifying the actual barrier heights as well developing methods to measure microscopic diversity within the protein folding ensemble.

In Figure 8, the position of each folding ensemble on the *y*-axis corresponds to the average apparent free energy ΔG (kcal/mol) of each folding ensemble—U, T_2, I, T_1, and N. The position on the *x*-axis displays the *m*-values (kcal/mol-[GdmCl]) of each of folding ensemble—U, T_2, I, T_1, and N. The *m*-value (*x*-axis) of each species is measured by the cumulative kinetic *m*-values preceding the species in the folding pathway. For example, the *m*-value and ΔG-value of T_1 are determined by

$$\Delta G_{T_1} = \Delta G_{UT_2}^{H_2O} - \Delta G_{IT_2}^{H_2O} + \Delta G_{IT_1}^{H_2O} \quad (21)$$

$$m_{T_1} = m_{UT_2} + m_{IT_2} + m_{IT_1} \quad (22)$$

In Figure 8, the *m*-value of each species can be used to determine the similarity of each IL-1β folding species to the native state, i.e., as the reaction coordinate (i.e., a variable which will linearly quantitate the amount of "nativeness"). The *m*-value is used as a reaction coordinate since it has been shown to correlate linearly with the physical property of ΔSASA between the native and unfolded states in proteins (*7*).

In Figure 8, free energy profiles at pH 5 and 7 illustrate that pH alters the thermodynamic stability ΔG (*y*-axis) of species on the pathway but does not significantly alter the *m*-values (*x*-axis). Thus, the ΔSASA of IL-1β does not appear to change significantly between pH 5 and 7 even though the thermodynamic stability is significantly changed. This finding is consistent with lack of change in the average fluorescence wavelength between pH 5−7 (Figure 1B) and secondary structure (*1*, *29*).

Transition state T_2 and T_1 ΔSASAs Are Highly Similar to the ΔSASAs of Macroscopic Folding Species I and N, Respectively. Properties of protein folding transition states are difficult to study due to the fact that, by definition, transition states do not significantly populate during folding. However, the ΔSASA of a transition state may be inferred by comparing the *m*-values of the transition state with the *m*-value of the native state. In simple two-state folding proteins, the parameter β^U is used to measure of the fraction of native ΔSASA in the transition state (*33*, *34*)

$$\beta^U = \frac{m_{\text{folding}}}{m_{\text{folding}} + m_{\text{unfolding}}} \tag{23}$$

The parameters m_{folding} and $m_{\text{unfolding}}$ are the kinetic *m*-values for folding and unfolding, respectively. By definition, $\beta^U = 0$ for the unfolded ensemble and $\beta^U = 1$ for the native state. In the case of a three-state folding protein, such as IL-1β, the measurement of β^U is complicated by multiple folding species (transition states T_2 and T_1, intermediate I). For a three-state folding protein, β^U for states T_2, I, and T_1 would be characterized through eqs 24−26:

$$\beta^U_{T_2} = \frac{m_{UT_2}}{m^{\text{kinetic}}_{NU}} \tag{24}$$

$$\beta^U_{I} = \frac{m_{UT_2} + m_{IT_2}}{m^{\text{kinetic}}_{NU}} \tag{25}$$

$$\beta^U_{T_1} = \frac{m_{UT_2} + m_{IT_2} + m_{IT_1}}{m^{\text{kinetic}}_{NU}} \tag{26}$$

In eqs 24−26, β^U measures the fraction of native ΔSASA each species. In two-state proteins, β^U is a straightforward measure of the transition state placement. Since two transitions exist in three-state proteins, each transition state must be normalized between the reactant and product of each folding step. To compare the transition state placement in three-state proteins, a parameter β^V is calculated for both folding transition states in a three-state protein. The U → I transition state, T_2, is characterized with the parameter $\beta^V_{T_2}$, calculated using eq 27:

$$\beta^V_{T_2} = \frac{m_{UT_2}}{m_{UT_2} + m_{IT_2}} \tag{27}$$

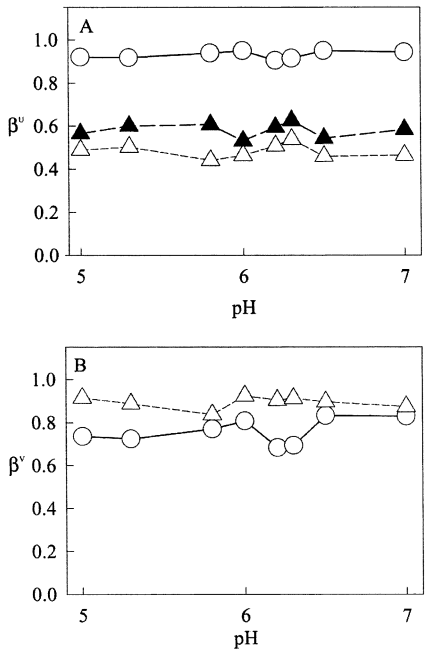

FIGURE 9: (A) β^U values of IL-1β folding species: transition state T_2, $\beta^U_{T_2}$ (--△--); intermediate I, β^U_I (--▲--); and transition state T_1, $\beta^U_{T_1}$ (−○−), relative to the native state. (B) β^V values of transition state T_2 relative to the U → I transition, $\beta^V_{T_2}$ (--△--), and transition state T_1 relative to the I → N transition, $\beta^U_{T_1}$ (−○−).

The I → N transition state, T_1, is characterized with the parameter $\beta^V_{T_1}$, calculated using eq 28:

$$\beta^V_{T_1} = \frac{m_{IT_1}}{m_{IT_1} + m_{NT_1}} \tag{28}$$

Figure 9A shows the values of β^U for IL-1β folding species T_2, I, and T_1 between pH 5−7. All values of $\beta^V_{T_2}$, β^U_I, and $\beta^U_{T_1}$ do not change significantly between pH 5−7, indicating the ΔSASA of transition states and intermediates in the IL-1β folding pathway do not change between pH 5−7. $\beta^U_{T_2}$ is 0.48 ± 0.17, indicating that approximately 50% of the native ΔSASA is buried in the early transition state T_2. β^U_I is 0.58 ± 0.17, a value consistent with the percentage of native signal from CD folding kinetics (*26*) and amide-hydrogen exchange protection (*5*). $\beta^U_{T_1}$ is 0.93 ± 0.094, indicating that 93% of native ΔSASA is buried at the later transition state T_1. Since the values of $\beta^U_{T_2}$, β^U_I, and $\beta^U_{T_1}$ are observed to be independent of pH, the reported error is determined at the 95% confidence interval using the values of $\beta^U_{T_2}$, β^U_I, and $\beta^U_{T_1}$ measured at each of the eight pH conditions (8 independent measurements of $\beta^U_{T_2}$, β^U_I, and $\beta^U_{T_1}$/7 degrees of freedom).

Figure 9B shows the values of β^V for IL-1β transition states T_2 and T_1 between pH 5−7. As with β^U in Figure 9A, the β^V parameters in Figure 9B do not change appreciably between pH 5 and 7. $\beta^U_{T_2}$ is 0.89 ± 0.15, indicating that transition state T_2 is highly similar to the intermediate I. $\beta^V_{T_1}$ is 0.76 ± 0.32, indicating that transition state T_1 is highly similar to the native state N. Since the values of $\beta^V_{T_2}$ and $\beta^V_{T_1}$ are observed to be independent of pH, the reported error is determined at the 95% confidence interval using the values of $\beta^V_{T_2}$ and $\beta^V_{T_1}$ measured at each of the eight

Table 1: Comparison of Three-State Folding Proteins with Respect to Various Parameters[a]

three-state protein (ref)	T_2			I		T_1	
	$\beta^U_{T_2}$	$\beta^V_{T_2}$	ln $k^{H_2O}_{UT_2}$	β^U_I	$\beta^U_{T_1}$	$\beta^V_{T_1}$	ln $k^{H_2O}_{IT_1}$
ubiquitin (*24*)	0.00	0.00	6.6	0.65	0.65	0.00	5.9
RNase A (*40*)	−	−	burst	0.45	0.47	0.05	4.8
CheY (*41*)	−	−	burst	0.69	0.77	0.25	3.1
Barnase (*42*)	−	−	burst	0.50	0.75	0.50	2.5
N-PGK (*43*)	−	−	burst	0.72	0.80	0.43	2.3
RNase H (*44*)	−	−	burst	0.58	0.80	0.52	−0.3
IL-1β	0.48 ± 0.17	0.89 ± 0.15	1.4	0.58 ± 0.17	0.93 ± 0.09	0.76 ± 0.32	−4.0

[a] Since, for IL-1β, parameters β^U and β^V are observed to be independent of pH, the reported error in m_{NU} for IL-1β is determined at the 95% confidence interval using the *m*-values measured at each of the 8 pH conditions (8 independent *m*-value measurements/7 degrees of freedom). Kinetic rates for IL-1β are reported at pH 7.0. All parameters for other proteins are determined from the values in the listed reference.

pH conditions (8 independent measurements of $\beta^V_{T_2}$ and $\beta^V_{T_1}$/ 7 degrees of freedom).

$\beta^V_{T_2}$ and $\beta^V_{T_1}$ for IL-1β can be compared to the β^V values of other proteins. Table 1 shows a comparison of three-state folding proteins with respect to the following parameters:

- $\beta^U_{T_2}$, the position of the transition state T_2 in the U → N folding pathway, where U is the unfolded ensemble and N is the native state. $\beta^U_{T_2} = 0$ indicates that T_2 has the same ΔSASA as U and $\beta^U_{T_2} = 1$ indicates that T_2 has the same ΔSASA as N.
- $\beta^V_{T_2}$, the position of the transition state T_2 in the U → I folding transition, where U is the unfolded ensemble and I is the partially folded intermediate ensemble. $\beta^U_{T_2} = 0$ indicates that T_2 has the same ΔSASA as U and $\beta^V_{T_2} = 1$ indicates that T_2 has the same ΔSASA as I.
- ln $k^{H_2O}_{UT_2}$, the natural log of the rate constant determined for the folding reaction:

$$U \xrightarrow{k^{H_2O}_{UT_2}} I$$

- β^U_I, the position of the intermediate I in the U → N folding pathway, where U is the unfolded ensemble and N is the native state. $\beta^U_I = 0$ indicates that I has the same ΔSASA as U and $\beta^U_I = 1$ indicates that I has the same ΔSASA as N.
- $\beta^U_{T_1}$, the position of the transition state T_1 in the U → N folding pathway, where U is the unfolded ensemble and N is the native state. $\beta^U_{T_1} = 0$ indicates that T_1 has the same ΔSASA as U and $\beta^U_{T_1} = 1$ indicates that T_1 has the same ΔSASA as N.
- $\beta^V_{T_1}$, the position of the final transition state T_1 in the I → N folding transition, where I is a partially folded intermediate populated in the folding of three-state proteins. $\beta^V_{T_1} = 0$ indicates that T_1 has the same ΔSASA as I and $\beta^V_{T_1} = 1$ indicates that T_1 has the same ΔSASA as N.
- ln $k^{H_2O}_{IT_1}$, the natural log of the rate constant determined for the folding reaction

$$I \xrightarrow{k^{H_2O}_{IT_2}} N$$

in three-state proteins.

Previous work has examined possible correlation between transition state placement, characterized by the parameter β^V, and folding rates in two-state folding proteins. High values of β^V have been shown to correlate with slower folding rates in model calculations and has been attributed to increased configurational entropy to the transition state free energy barrier at higher values of β^V (*35*). However, the apparent folding rate constant, k^{H_2O}, in two-state proteins was found to be only loosely correlated with β^V and was been shown to be better correlated with the parameter of contact order (*36*).

In this study, IL-1β has been shown to be a three-state folding protein. Therefore, the most appropriate parameter comparison is between IL-1β and other three-state folding proteins (shown in Table 1). In all three-state proteins except IL-1β, the initial transition, U → I equilibrates within the dead time of stopped flow mixing. In the case of ubiquitin, submillisecond kinetics have been quantitated with fitting methods and can be used for comparison to IL-1β. Although the comparison of the U → I reaction in three-state proteins consists of only these two proteins, there are notable differences between them. The fast folding ubiquitin (ln $k^{H_2O}_{UT_2}$ = 6.6) has a transition state, T_2, highly similar to the unfolded ensemble, U, as indicated by the parameter $\beta^V_{T_2}$ = 0.0. The slow folding IL-1β (ln $k^{H_2O}_{UT_2} = 1.4$) has a transition state, T_2, highly similar to the intermediate, I, as indicated by the parameter $\beta^V_{T_2} = 0.89$. This observation suggests that high $\beta^V_{T_2}$ values may result in slower U → I folding in three-state proteins.

All values of β^U_I for the intermediate I in the three-state proteins suggest that the intermediate typically possesses 50−70% of native state ΔSASA, as does IL-1β (55%). Thus, the degree of folding in the folding intermediate is consistent across this set of three-state proteins. To address the I → N transition state, T_1, it is noteworthy that the IL-1β parameter, $\beta^V_{T_1} = 0.76$, is the highest of all three-state proteins and the rate, $k^{H_2O}_{IT_1}$, is the slowest. Unlike the poor correlation reported for two-state proteins (*36*), a good linear correlation is found between $\beta^V_{T_1}$ and ln $k^{H_2O}_{XT_1}$ in three-state proteins ($R^2 = 0.90$). Thus, transition state placement appears to correlate with slow I → N folding in three-state proteins.

Comparison of IL-1β to Other β-Trefoil Proteins. Contact order has been shown to correlate with the folding rates of two-state folding proteins. For this reason, comparing the folding properties of proteins which have similar contacts order can elucidate the extent to which contact order defines folding rates and pathways. If contact order entirely defined protein folding, all members of a structural family would

Table 2: Folding Properties Measured for Each β-Trefoil Protein[a]

	intermediates		rates (s^{-1})[b]		transition states[b]	
protein (refs)	kinetics[b]	early strands[c]	ln $k_{Fast}^{H_2O}$	ln $k_{Slow}^{H_2O}$	$\partial\beta_T^V/\partial$pH	$\partial m_{NT_X}/\partial$[D][d]
hisactophilin (*13*, *14*)	1−2 exp	4−8	5.8	1.1	0.0 ± 0.0	$m''_{NT_X} = 0.0473$
aFGF (*11*)	2 exp	1, 12	2.0	−3.8	?	$m''_{NT_X} \sim 0$
BFGF (*12*)	2 exp	?	−2.3	−7.0	?	$m''_{NT_X} \sim 0$
IL-1β (*3*−*5*)	2 exp	6−10	1.4	−4.0	$\beta_{T_2}^V$ 0.00 ± 0.04	$m''_{NT_X} = 0.0027 \pm 0.050$
					$\beta_{T_1}^V$ 0.04 ± 0.07	

[a] Errors listed are 95% confidence intervals based on measurements at all pH conditions. [b] Parameters were measured from monitoring tryptophan fluorescence as a probe. In the case of hisactophilin, rate ln $k_{Slow}^{H_2O}$ is estimated from the most stable conditions (pD 7.8, D_2O), where the intermediate appears to be populated (two exponential kinetics). Listed values of ln $k_{Fast}^{H_2O}$ and ln $k_{Slow}^{H_2O}$ are not determined rigorously from global fitting but from direct extrapolation of the fitted rate constants to 0 M GdmCl and therefore may differ slightly from those reported in the reference. [c] Early strands are determined from the earliest strands demonstrating significant hydrogen−deuterium exchange protection. [d] Coefficient m''_{NT_X} reflects a linear dependence of the denaturant sensitivity parameter m_{NT_X} on denaturant through the equation $m_{NT_X} = m'_{NT_X} + m''_{NT_X}$[D].

fold at the similar rates with the same basic pathway mechanism.

Although the folding of β-trefoil proteins appear to share some properties in common, they are by no means completely similar. Table 2 lists a number of folding properties measured for each β-trefoil protein. From Table 2, certain properties appear to be conserved among the β-trefoil proteins studied, although there are clear exceptions. Experimental conditions can be found for each protein where folding kinetics, monitored by tryptophan fluorescence, are best fit with a biexponential function. The degree to which a basic mechanism is conserved is unclear, since the number of exponentials required to fit the folding kinetics can change depending on the experimental probe used and protein stability during the measurements (*11*−*14*). Nonetheless, discrete transient intermediates appear to consistently populate in the folding of β-trefoil proteins. However, the structural properties of these transient intermediates also appear to be inconsistent. For example, in IL-1β and hisactophilin, the intermediate demonstrates hydrogen exchange protection in the central strands while, in aFGF, early hydrogen exchange protection is observed at the N and C termini.

The relatively slow rate of folding observed for both $k_{Fast}^{H_2O}$ and $k_{Slow}^{H_2O}$ of IL-1β is also shared among the other β-trefoil proteins. Hisactophilin, at pH 7.8 in D_2O, is the exception as it is an order of magnitude faster than the other β-trefoil proteins for both $k_{Fast}^{H_2O}$ and $k_{Slow}^{H_2O}$. Regardless, hisactophilin is still considered a slow folder compared to the three-state proteins described in Table 1. Thus, the β-trefoil topology does appear to result in slow folding in the proteins studied thus far.

The data in Table 1 indicates that high β_T^V values correlate with slow folding rates in three-state proteins. Due to the fact that β_T^V values are not reported for the individual steps U → I and I → N in the other β-trefoil proteins, a comparison of β_T^V within this structural family cannot be made yet. A value of $\beta_T^V = 0.71$ is reported for hisactophilin assuming a two-state, not three-state, folding model and is therefore not directly comparable to IL-1β parameters $\beta_{T_2}^V$ and $\beta_{T_1}^V$.

Despite this fact, the features of the transition state ensemble can be probed by determining if β_T^V changes significantly at different stabilities ΔG_{NU} ($\partial\beta_T^V/\partial\Delta G_{NU}$). If $\partial\beta_T^V/\partial\Delta G_{NU}$ is observed, it has been attributed to shifting populations of different high-energy transition state configurations across different stability conditions (*37*). If $\partial\beta_T^V/\partial\Delta G_{NU}$ is not observed, it has been attributed to an ensemble of high energy transition state configurations which dominate under all stability conditions (*37*). Thus, low value of $\partial\beta_T^V/\partial\Delta G_{NU}$ is indicative of a "robust" ensemble of high-energy transition state configurations.

One probe of the high-energy transition state robustness is $\partial\beta_T^V/\partial$pH, a parameter reported for both IL-1β and hisactophilin. In both proteins, $\partial\beta_T^V/\partial$pH is either zero or small enough to be statistically insignificant, indicating that the transition state position does not move significantly when the stability is altered by pH shifts. This behavior has been attributed to a landscape where a limited set of high-energy transition state configurations occupy the transition state regardless of varying stability. It should be noted that $\partial\beta_T^V/\partial$pH only probes the high-energy transition state configurations which are destabilized by pH shifts (i.e., electrostatic interactions).

Another method used to examine the high-energy transition state robustness is quantifying curvature, m''_{NT_X}, in the slope of the unfolding kinetic parameter, log k_{NT_X}, versus denaturant concentration [D] through eq 29:

$$\log k_{NT_X} = \log k_{NT_X}^{H_2O} + \frac{m''_{NT_X}}{2.303RT}[D] - \frac{m''_{NT_X}}{2.303RT}[D]^2$$

The subscript T_X in the variable k_{NT_X} refers to the transition state immediately preceding the native state in the folding pathway of each protein, which is typically the transition state probed in unfolding experiments. Although hisactophilin unfolding by urea clearly demonstrates curvature ($m''_{NT_X} = 0.0473$), this curvature is not observed in other β-trefoil proteins. IL-1β unfolding by GdmCl does not indicate significant curvature as evidenced by the parameter $m''_{NT_X} = 0.0027 \pm 0.05$. Although values of m''_{NT_X} are not directly calculated for aFGF and bFGF, visual inspection of aFGF/bFGF unfolding kinetics does not reveal significant curvature.

The comparisons between β-trefoil proteins indicate three important findings. [1] The high-energy transition state robustness of hisactophilin is lower for denaturant than pH, while IL-1β transition state appears to be robust during either perturbation. [2] The high-energy transition state robustness

of hisactophilin may be lower than other β-trefoil proteins, possibly accounting for its faster folding rate. [3] Although similarities exist, the folding rate, early intermediate structures, and transition state robustness of β-trefoil proteins are not determined exclusively by either structural topology or contact order. This fact has also been observed in folding studies of other structural protein families (*38*, *39*) and suggests that, while topology and contact order are important determinants of protein folding, they are by no means the only relevant factors.

Conclusions. Interleukin-1β is an all β-sheet protein which undergoes a 3.5 kcal/mol increase in stability as pH is decreased from 7 to 5. The predominant native stability changes between pH 5−7 result from changes in the folding, not unfolding, free energy barriers. The GdmCl sensitivity parameters, i.e., *m*-values, for all folding species measured in the interleukin-1β folding pathway are unchanged between pH 5−7, indicating that the same high-energy transition state ensemble limits each transition regardless of varying stability.

Kinetic and equilibrium folding analysis of interleukin-1β between pH 5−7 indicates that interleukin-1β is well characterized with a sequential three-state mechanism

$$U \underset{k_{IT_2}}{\overset{k_{UT_2}}{\rightleftharpoons}} I \underset{k_{NT_1}}{\overset{k_{IT_1}}{\rightleftharpoons}} N$$

Unlike other three-state proteins studied to date, all kinetic transitions of IL-1β are directly measurable with stopped flow methods. An important aspect of IL-1β folding is that the ΔSASA of early transition state ensemble T_2 is highly similar to the ΔSASA of the intermediate ensemble I. Also, the ΔSASA of the later transition state T_1 is highly similar to the ΔSASA of the native state N. Compared to other three-state proteins, IL-1β folds at a much slower rate and has a much more nativelike transition state. These results are supportive of the hypothesis that native state topologies which restrict a protein to adopt nativelike transition states result in slower experimentally measured folding rates.

Although exceptions do exist, many of the folding properties of IL-1β are shared among other β-trefoil proteins. This indicates that, in β-trefoil proteins, structural topology is a dominant, but not absolute, predictor of folding behavior.

ACKNOWLEDGMENT

We thank Joe Adams for the use of his stopped-flow fluorimeter, Elaine Yang for help with IL-1β purification and kinetic studies, and Osman Bilsel for providing SAVUKA kinetic analysis software.

REFERENCES

1. Craig, S., Schmeissner, U., Wingfield, P., and Pain, R. H. (1987) *Biochemistry 26*, 3570−3576.
2. Chrunyk, B. A., Evans, J., and Wetzel, R. (1993) in *Protein Folding In Vivo and In Vitro* (Cleland, J. L., Ed.) pp 46−58, American Chemical Society, Washington, DC.
3. Varley, P., Gronenborn, A. M., Christensen, H., Wingfield, P. T., Pain, R. H., and Clore, G. M. (1993) *Science 260*, 1110−3.
4. Finke, J. M., Roy, M., Zimm, B. H., and Jennings, P. A. (2000) *Biochemistry 39*, 575−83.
5. Heidary, D. K., Gross, L. A., Roy, M., and Jennings, P. A. (1997) *Nat. Struct. Biol. 4*, 1−10.
6. Clementi, C., Jennings, P. A., and Onuchic, J. N. (2000) *Proc. Natl. Acad. Sci. U.S.A. 97*, 5871−6.
7. Myers, J. K., Pace, C. N., and Scholtz, J. M. (1995) *Protein Sci 4*, 2138−48.
8. Roder, H., and Shastry, M. R. (1999) *Curr. Opin. Struct. Biol. 9*, 620−6.
9. Park, S. H., Shastry, M. C., and Roder, H. (1999) *Nat. Struct. Biol. 6*, 943−7.
10. Kuwata, K., Shastry, R., Cheng, H., Hoshino, M., Batt, C. A., Goto, Y., and Roder, H. (2001) *Nat. Struct. Biol. 8*, 151−5.
11. Samuel, D., Kumar, T. K., Balamurugan, K., Lin, W. Y., Chin, D. H., and Yu, C. (2001) *J. Biol. Chem. 276*, 4134−41.
12. Estape, D., and Rinas, U. (1999) *J. Biol. Chem. 274*, 34083−8.
13. Liu, C., Gaspar, J. A., Wong, H. J., and Meiering, E. M. (2002) *Protein Sci. 11*, 669−79.
14. Houliston, R. S., Liu, C., Singh, L. M., and Meiering, E. M. (2002) *Biochemistry 41*, 1182−94.
15. Meyers, C. A., Johanson, K. O., Miles, L. M., McDevitt, P. J., Simon, P. L., Webb, R. L., Chen, M.-J., Holskin, B. P., Lillquist, J. S., and Young, P. R. (1987) *J. Biol. Chem. 262*, 11176−11181.
16. Gill, S. C., and von Hippel, P. H. (1989) *Anal. Biochem. 182*, 319−326.
17. Eftink, M. R. (1994) *Biophys. J. 66*, 482−501.
18. Raschke, T. M., and Marqusee, S. (1997) *Nat. Struct. Biol. 4*, 298−304.
19. Pace, C. N. (1986) *Methods Enzymol 131*, 266−80.
20. Schellman, J. A. (1987) *Biopolymers 26*, 549−59.
21. Marquardt, D. W. (1963) *J. Soc. Ind. Appl. Math. 11*, 431−441.
22. Bevington, P. R. (1969) *Data Reduction and Error Analysis For the Physical Sciences*, Vol. 1, McGraw-Hill, New York.
23. Bernasconi, C. F. (1976) *Relaxation Kinetics*, Academic Press, New York.
24. Khorasanizadeh, S., Peters, I. D., and Roder, H. (1996) *Nat. Struct. Biol. 3*, 193−205.
25. Finke, J. M., Gross, L. A., Ho, H. M., Sept, D., Zimm, B. H., and Jennings, P. A. (2000) *Biochemistry 39*, 15633−42.
26. Finke, J. M., and Jennings, P. A. (2001) *J. Biol. Phys. 27*, 119−131.
27. Finn, B. E., Chen, X., Jennings, P. A., Saalau-Bethel, S. M., and Matthews, C. R. (1992) in *Protein Engineering − A Practical Approach* (Rees, A. R., Wetzel, R., and Sternberg, J. E., Eds.) pp 167−189, JRL Press, Oxford.
28. Roder, H., and Colón, W. (1997) *Curr. Opin. Struct. Biol. 7*, 15−28.
29. Clore, G. M., and Gronenborn, A. M. (1991) *J. Mol. Biol. 221*, 47−53.
30. Wetzel, R., and Chrunyk, B. A. (1994) *FEBS Lett. 350*, 245−248.
31. Chrunyk, B. A., Evans, J., Lillquist, J., Young, P., and Wetzel, R. (1993) *J. Biol. Chem. 268*, 18053−18061.
32. Jackson, S. E., and Fersht, A. R. (1991) *Biochemstry 30*, 10428−10435.
33. Tan, Y. J., Oliveberg, M., and Fersht, A. R. (1996) *J. Mol. Biol. 264*, 377−89.
34. Luisi, D. L., and Raleigh, D. P. (2000) *J. Mol. Biol. 299*, 1091−100.
35. Doyle, R., Simons, K., Qian, H., and Baker, D. (1997) *Proteins 29*, 282−91.
36. Plaxco, K. W., Simons, K. T., and Baker, D. (1998) *J. Mol. Biol. 277*, 985−94.
37. Oliveberg, M., Tan, Y. J., Silow, M., and Fersht, A. R. (1998) *J. Mol. Biol. 277*, 933−43.
38. Burns, L. L., Dalessio, P. M., and Ropson, I. J. (1998) *Proteins 33*, 107−18.
39. Ferguson, N., Capaldi, A. P., James, R., Kleanthous, C., and Radford, S. E. (1999) *J. Mol. Biol. 286*, 1597−608.
40. Houry, W. A., Rothwarf, D. M., and Scheraga, H. A. (1995) *Nat. Struct. Biol. 2*, 495−503.
41. Lopez-Hernandez, E., Cronet, P., Serrano, L., and Munoz, V. (1997) *J. Mol. Biol. 266*, 610−20.
42. Oliveberg, M., and Fersht, A. R. (1996) *Biochemistry 35*, 2726−37.
43. Parker, M. J., Spencer, J., and Clarke, A. R. (1995) *J. Mol. Biol. 253*, 771−86.
44. Raschke, T. M., Kho, J., and Marqusee, S. (1999) *Nat. Struct. Biol. 6*, 825−31.

BI026197K